Journal of Marine Science and Application (2026) 25: 1349-1363
https://doi.org/10.1007/s11804-026-00794-w

RESEARCH ARTICLE

Flight Trajectory Design and Simulation Analysis of a High-Altitude, Long-Distance Gliding UUV

Chiyu Wang[1], Zhiming Qiu[1,2], Zhaoyong Mao[1,3,4], Peiyu Chen[5], Fengtianyi Huang[1,6], Yajun Chai[1], Yuxian Yang[1] and Wenjun Ding[1,3,4]

Received: 01 March 2025 / Accepted: 22 November 2025
© Harbin Engineering University and Springer-Verlag GmbH Germany, part of Springer Nature 2026

Abstract

To enhance the long-distance penetration and combat capabilities of unmanned underwater vehicles (UUVs), this study proposes a high-altitude, long-distance gliding UUV that can be rapidly deployed by a penetration platform. According to the overall scheme, the overall trajectory is partitioned into five distinct stages: the flight stage of the penetration platform, the release stage, the conversion stage, the glide stage, and the water entry stage of the gliding UUV, with trajectory characteristics discussed for each operational segment. UUV conversion, after its release from the penetration platform, is accomplished by designing a piecewise quadratic trajectory inclination angle. The feasibility of the conversion stage trajectory design is validated using a RHC algorithm. The influence of different initial velocities on UUV conversion is also investigated. The glide stage employs a reverse thrust methodology to ensure water entry safety. Trajectory characteristics in the five different stages are studied, with the simulation verifying the rationality of the overall trajectory. Accordingly, the UUV achieves a total flight range of 410 km within 633.5 s, with the designed trajectory enabling smooth conversion and high-altitude glide performance. The water entry velocity of the UUV is 33.3 m/s, and the water entry angle is −72°, meeting the requirements of load shedding on UUVs. The reasonably designed trajectory of the high-altitude, long-distance gliding UUV establishes a foundation for subsequent engineering validation.

Keywords Penetration; Unmanned underwater vehicle; High-altitude; Long-distance gliding; Flight trajectory; Smooth conversion

1 Introduction

The future battlefield is expected to be dominated by unmanned combat systems, with unmanned underwater vehicles (UUVs) serving as key assets in underwater warfare. The UUV technology, characterized by long range, strong penetration capability, good maneuverability, reduced detectability, and effective trans-medium water entry attacks, is projected to become the mainstream direction of future development (Wang et al., 2024a; Yao et al., 2023; Zhao et al., 2024).

Gliding UUVs launched via rockets exhibit characteristics such as flexible deployment and launch capabilities, high flight speed, extended flight range, and strong maneuverability for penetration (Ding et al., 2020; Tang et al., 2025). These features enable them to rapidly engage various long-range targets and perform auxiliary military missions, including surveillance, reconnaissance, and precision strikes (Zhao et al., 2020). Consequently, they have become a prominent research focus in the field of aerospace engineering (Qi et al., 2022). Penetration platforms undergo ignition and boost during the initial flight stage, subsequently transitioning into a passive flight stage. Throughout this process, the flight trajectory of the penetration platform represents one of the critical technologies in rocket-assisted launches. It is directly correlated with the flight performance of the rocket as a carrier platform

Article Highlights

- In order to improve the long-range penetration and combat capability of the trans-media aircraft, a scheme of rapid deployment of the trans-media aircraft by rocket launching is proposed.
- The safe conversion of the aircraft after separation from the rocket is achieved by designing a two-stage trajectory inclination angle method.
- The glide stage is designed and the way of rocket reverse thrust is adopted to meet the aircraft's safe water entry requirements.

✉ Wenjun Ding
dingwenjun@nwpu.edu.cn

[1] Unmanned System Research Institute, Northwestern Polytechnical University, Xi'an 710072, China

[2] Naval Research Academy, Beijing 100161, China

[3] National Key Laboratory of Unmanned Aerial Vehicle Technology, Xi'an 710072, China

[4] Integrated Research and Development Platform of Unmanned Aerial Vehicle Technology, Xi'an 710072, China

[5] Beijing Aerospace Automatic Control Institute, Beijing 100854, China

[6] School of Automation, Northwestern Polytechnical University, Xi'an 710072, China

for penetration (Guo et al., 2024a).

During flight, rockets can reach altitudes of tens of kilometers. Given their static instability, strong nonlinearity, and uncertainties in aerodynamic parameters (Yang and Xia, 2020), the design of a rational trajectory is of paramount importance (Yılmaz and Cihan, 2023). Upon a rocket's launch into a target area, gliding UUVs can be deployed. This enables rapid aerial deployment and maintains high concealment after water entry (Zhang et al., 2021). UUVs can collaborate with underwater submarines in alphabetic combat formations, exchange information, and participate in cross-domain mission coordination (Wei et al., 2023) with surface vessels and unmanned aerial vehicles (UAVs) (Wang et al., 2024b; Xu and Guedes Soares, 2025; Yan et al., 2025; Ye et al., 2023). Furthermore, trajectory design and planning constitute essential components of an aircraft mission planning system, significantly enhancing the operational capabilities of military aircraft (Chen et al., 2024). Currently, numerous methods are available to correct planned trajectories to ensure accuracy, including various artificial intelligence approaches (Ahmed and Sheltami, 2024; Chen et al., 2025a; Hu et al., 2025a, 2025b; Lui et al., 2023; Yahi et al., 2024).

High-altitude, long-distance gliding UUVs encompass multiple stages, including rocket flight, UUV release, conversion, aerodynamic glide, and water entry. Accordingly, rational trajectory design and planning are required to coordinate these five distinct flight stages. Currently, there are several relevant studies on rocket-assisted vehicles and high-altitude gliding UUVs. For instance, Fan et al. (2022) used the time and frequency domains to identify four air rudder models of boost-glide aircraft. Hu et al. (2025) proposed a maneuver mode parametric modeling method based on trajectory curve evolution laws to characterize maneuver modes in hypersonic vehicle defense. Guo et al. (2024b) presented an integrated decision-making and control framework for morphing flight vehicles with variable-span wings in the glide phase. This decision-making method was designed to optimize comprehensive performance indices, including the lift-to-drag ratio and attitude tracking effect, thus ensuring physical realizability. Chen et al. (2025b) focused on how trans-medium glide functions influence the design of the glider's air track by analyzing the relationship between the start and end states of air glide, lift-to-drag ratio, and range. Liu et al. (2014) investigated the aerodynamic configuration of a high-altitude gliding UUV and performed numerical simulations. Liu and Bai (2021) analyzed the impact of high-altitude wind direction on dynamic gliding by simulating a six-degree-of-freedom model. Pan et al. (2012, 2013, 2009) simulated and analyzed the entire trajectory of a high-altitude gliding UUV, focusing on the low-altitude penetration phase and the deceleration phase. They employed two deceleration strategies—isometric control and rocket reverse thrust—to achieve rapid penetration and controlled deceleration during water entry, respectively. Chen et al. (2020) designed a high-altitude glide torpedo trajectory based on an optimal guidance law, enabling trajectory inclination control during wing separation. Zhang et al. (2013) and Wang et al. (2012) developed and simulated control strategies for long-distance, high-altitude gliding UUVs. Li (2017) proposed a specific design for rocket-borne UAVs, optimizing the rocket's flight trajectory. However, the post-release UUV conversion was not addressed in their study.

Although prior research has explored rocket-launched aircraft and high-altitude gliding UUVs, holistic investigations of complete flight trajectories—spanning from the penetration platform launch to UUVs' aquatic deployment—remain scarce. Existing studies have predominantly focused on isolated phases, such as the rocket launch stage or the UUV water entry stage, and provide minimal discussions of how to achieve rapid and stable conversion under extreme angles and attitudes after UUV separation from the penetration platform. To address this gap, this study proposes a rocket-launched rapid deployment scheme for high-altitude, long-distance gliding UUVs, accompanied by a comprehensive flight trajectory framework integrating five distinct operational stages. Leveraging established configurations of a penetration platform (Zhang, 2010) and a gliding UUV (Li, 2018) from published literature, this work systematically analyzes trajectory characteristics across all stages while identifying technical challenges and mission requirements for each stage. Safe UUV conversion after its separation from the rocket is achieved by designing a piecewise quadratic trajectory inclination angle. The rationality of trajectory planning for the UUV conversion stage is emphatically examined, with planned trajectory execution achieved through the implementation of a RHC algorithm. During the water-entry stage, a miniature rocket reverse thrust system is employed for drag reduction, enabling the UUV's seamless medium transition. This approach keeps the impact velocity and water-entry angle within optimal thresholds, thus meeting dual requirements for structural load mitigation and safe aquatic ingress.

2 Overall flight plan for a high-altitude, long-distance gliding UUV

2.1 Complete flight scheme of the high-altitude, long-distance gliding UUV

The overall flight scheme of the high-altitude, long-distance gliding UUV is shown in Figure 1. The proposed system equips a conventional UUV with extended-range glider and rocket booster components with control and guidance functions. These components are placed inside

the rocket in a variable configuration by folding the wings. Using an existing small rocket as a penetration platform, the rocket can be launched into the air using a boosting engine. After a lift-off period, the boosting engine is shut down, and the rocket then moves passively. Upon reaching the desired area, the rocket deploys an internal deceleration device to reduce its velocity and then enters the release stage. The gliding UUV can quickly penetrate hundreds of kilometers in a few minutes after launching the rocket.

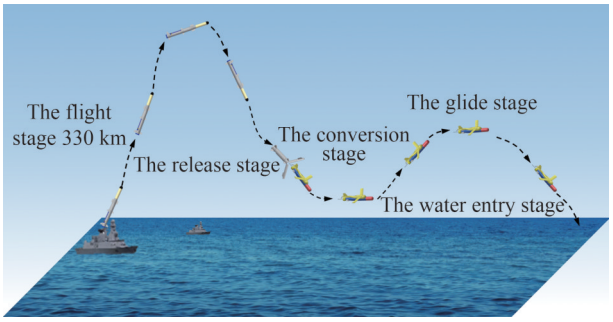


Figure 1 Flight process of the high-altitude, long-distance gliding UUV

At the end of the release stage, the gliding UUV is released from the inside of the rocket. Its folded wings are then deployed, initiating the conversion stage. During this phase, the gliding UUV can adjust its attitude in time by regulating the trajectory inclination angle, pulling the gliding UUV to level flight from the diving condition in preparation for the glide stage. After stabilizing the attitude in the glide stage, the trajectory of the gliding UUV passes into the water entry stage. The UUV crosses from air into water at an appropriate pitch angle and velocity for a particular strike or reconnaissance mission.

2.2 Trajectory characteristics during different flight stages

The proposed framework comprises five stages: the rocket's flight stage, the release stage, the conversion stage, the glide stage, and the water entry stage of the gliding UUV.

1) Flight stage: This stage is divided into two stages. One is the active flight stage with ignition, and the other is the passive flight stage during engine shutdown after a period of ignition. The entire rocket flight stage is roughly a projectile motion, which can quickly send the UUV to the target position. During this stage, the rocket's flight time, penetration range, and terminal altitude must be accounted for. The designed trajectory must be capable of covering sufficient distance within the specified time to meet the long-range penetration requirements. The terminal flight altitude significantly influences the trajectory during the release stage.

2) Release stage: After reaching its target area, the rocket activates the deceleration device, adjusting the velocity and the altitude to an appropriate value. Then, the gliding UUV separates from the rocket and enters the conversion stage. The terminal trajectory parameters of the rocket flight stage are similar to the initial parameters of the gliding UUV conversion stage, which significantly impact the conversion of the UUV. In the design process, the flight time of the rocket during the release stage must be accounted for. This parameter critically influences the UUV's release velocity, altitude, and trajectory inclination angle. Thus, the optimal selection of the release time is essential to facilitate enhanced conversion of the gliding UUV.

3) Conversion stage: This stage is the key point in the whole combat process of the high-altitude long-distance gliding UUV. First, the gliding UUV dives vertically, with both the pitch angle and trajectory inclination angle approaching $-90°$. Under the control of the designed trajectory program, the attitude of the gliding UUV is continuously adjusted and gradually transformed into a stable-level flight condition. Continuous adjustments to the vehicle's flight attitude must be considered during this stage. In the initial conversion stage, while the gliding UUV is in vertical descent, the altitude must not fall below the minimum safe level. Concurrently, the stabilized final altitude must not be excessive to prevent exceeding the vehicle's operational ceiling. Appropriate design parameters and control strategies are required to achieve a smooth recovery maneuver.

4) Glide stage: This stage ensures steady-state flight conditions such that the terminal altitude and velocity satisfy the requirements for the water entry stage. Before water entry, the gliding UUV glides continuously at an approximate fixed pitch angle, and its altitude and velocity gradually decrease during the glide stage.

5) Water entry stage: The UUV must enter the water within structurally permissible angles and velocity limits to prevent internal component damage, structural failure, or functional impairment. When the gliding UUV reaches the corresponding altitude, a miniature rocket reverse thrust system is activated to decrease the UUV's velocity sharply. This ensures that its pitch angle and velocity are within a reasonable range to meet the load-shedding requirements while entering the water.

2.3 Overall parameters of the rocket and gliding UUV

The dispersion accuracy requirements of UUVs for penetration launch platforms are relatively low, and the research on rocket launch trajectory is well-established. In this article, the rocket model is simplified as follows:

1) Throughout the entire flight of the rocket, it always moves in the longitudinal plane and is regarded as a particle.

2) The shape and mass distribution of the projectile are axisymmetric, and the thrust is along the axis of the

projectile.

3) Standard meteorological conditions are assumed, and wind disturbances are not considered.

4) The rocket is only affected by thrust, gravity, and resistance.

Relevant rocket parameters are given by the overall design department. The parameters required for trajectory simulation are given in Table 1 (Zhang, 2010). The parameters, including the drag coefficient, are also in the literature.

Table 1 Relevant parameters of the rocket

Full load mass (kg)	Fuel mass flow (kg/s)	Ignition time (s)	Exhaust velocity (m/s)	Reference area (m^2)
2 200	60	30	2 400	0.45

The three-dimensional model of the gliding UUV is illustrated in Figure 2, and the detailed overall parameters are presented in Table 2 (Li, 2018). The gliding UUV comprises two integrated subsystems: a folding-wing assembly analogous to fixed-wing UAV configurations featuring an aft-mounted propeller and a primary UUV body arranged in an underslung configuration beneath the wing structure. The wings are folded when the gliding UUV is unreleased and placed inside the rocket.

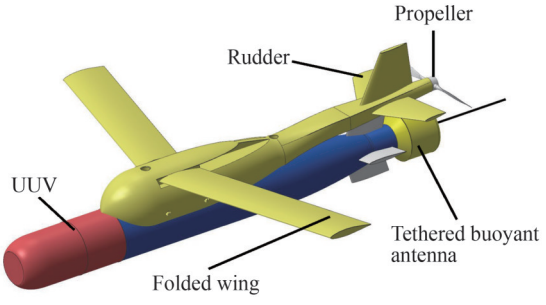


Figure 2 Three-dimensional model of the gliding UUV

The rocket is slowed down by a deceleration device during the release stage (Zhang, 2010). This device consists of four deceleration brakes. Each brake is fixed at the rear end of the rocket through root support. The overall drag coefficient is related to the flight Mach number. Upon entering the conversion stage, concurrent propeller activation generates auxiliary thrust to modulate the gliding UUV's trajectory. During the flight stages, the target trajectory is achieved by controlling the rudder angle. After entering the water, the tethered buoyant antenna at the tail

Table 2 Gliding UUV's wing parameters

Parameter	Glider	Horizontal tail	Vertical tail
Airfoil profile	NACA64A2-15	NACA0012-64	NACA0012-64
Relative thickness	0.15	0.12	0.12
Lift line slope (°)	0.12	0.125	0.125
Zero lift angle of attack (°)	−1.66	0	0
Angle of attack when the lift line deviates from linearity (°)	11	11.5	11.5
Maximum lift coefficient	1.5	1.5	1.5
Angle of attack corresponding to the maximum lift coefficient (°)	15	15	15
Pressure center	0.26	0.265	0.265
Zero-lift moment coefficient	0.06	0	0
Minimum resistance coefficient	0.004 3	0.005 6	0.005 6
Area (m^2)	0.831 9	0.174 6	0.092 2
Span (m)	2.884 3	0.665 4	0.303 8
Average aerodynamic chord length (m)	0.288 4	0.250 2	0.314 9
Aspect ratio	10	3	2
Wing root chord length (m)	0.288 4	0.295 7	0.405
Tip chord (m)	0.288 4	0.147 6	0.202 5
Taper ratio	1	0.5	0.5
Leading edge sweep angle (°)	15	30	30
Anhedral (°)	0		
Mounting angle (°)	1.67	–	–
Horizontal distance between the aerodynamic center and the gliding UUV's center of gravity (mm)	0	1 600	1 517
Distance between the chord plane and the horizontal axis plane (mm)	305	230	
Tail capacity	–	0.8	0.6
Deflection angle range (°)	–	−25–+25	−25–+25

of the UUV floats on the surface and receives command information.

This paper models the gliding UUV in the ballistic coordinate system, focusing on its flight characteristics within the vertical plane. The ballistic coordinate system is shown in Figure 3. The origin O of the ballistic coordinate system is located at the center of mass of the gliding UUV. The Ox-axis coincides with the velocity vector $\boldsymbol{V}$ of the gliding UUV center of mass, whereas the Oy-axis lies in the vertical plane containing the velocity vector $\boldsymbol{V}$ and is perpendicular to the Ox-axis.

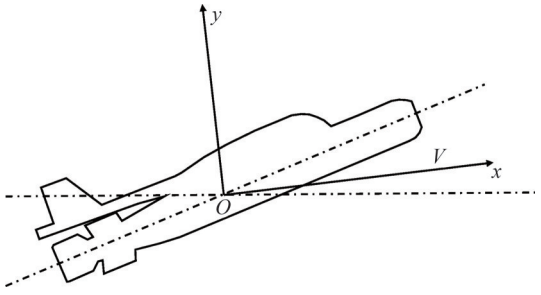


Figure 3 Coordinate system of the gliding UUV

The parameters for the trajectory of the gliding UUV are obtained through numerical simulation and verified by wind tunnel experiments. These parameters are presented in Table 3 (Li, 2018). The thrust values of the gliding UUV at different altitudes and velocities are shown in Table 4 (Li, 2018).

3 Trajectory simulation model of the high-altitude, long-distance gliding UUV

3.1 Dynamic model of the rocket in the flight stage

In the flight stage, the rocket primarily serves as a penetration carrier platform to quickly transport the gliding UUV to the target area. Because of the low positional precision requirement, no control trajectory or a simple program-controlled trajectory method is used to reduce cost. From the flight profile mission perspective of the high-altitude, long-distance gliding UUV, the trajectory design is mainly focused on the longitudinal plane. During dynamic modeling, this study focuses on the centroid motion equation of the rocket in the longitudinal plane with the surface curvature and altitude variation. To improve the accuracy of the calculation, the equation of motion accounts for the influence of the Earth's radius and changes in gravity. The relevant equations are given as follows:

$$\begin{cases} \dfrac{\mathrm{d}v_r}{\mathrm{d}t} = a_P - a_X - g_r \sin\theta_r \\ \dfrac{\mathrm{d}\theta_r}{\mathrm{d}t} = -\dfrac{g_r \cos\theta_r}{v_r} + \dfrac{v_r \cos\theta_r}{r_E + y_d + h_r} \\ \dfrac{\mathrm{d}R_r}{\mathrm{d}t} = v_r \cos\theta_r \left(1 + \dfrac{h_r}{r_E + h_d}\right)^{-1} \\ \dfrac{\mathrm{d}h_r}{\mathrm{d}t} = v_r \sin\theta_r \\ g_r = g_o \left(\dfrac{r_E}{r_E + h_d + h_r}\right)^2 \\ a_P = \dfrac{|\dot{m}_r|}{m_r} u_e + \dfrac{P_0 - P_r}{m_r} S_a \\ a_X = \dfrac{1}{2} \rho {v_r}^2 C_{Xr} S_r / m_r \\ m_r = m_0 - \int_0^t \dot{m}_r(t)\,\mathrm{d}t \end{cases} \tag{1}$$

where r represents rocket parameters; v is the velocity of the rocket; a_P is the acceleration produced by thrust; a_X represents acceleration produced by drag; θ is the trajectory inclination angle; g is the gravitational acceleration of the rocket; r_E represents the Earth's radius; h_d is the altitude of the rocket launch; h is the altitude of the rocket; x

Table 3 Relevant parameters of the gliding UUV

Ma	0.3	0.4	0.5	0.6	0.7	0.8
Lift line slope	4.88	4.98	5.12	5.31	5.65	5.99
Lift coefficient at zero angle of attack	0.14	0.15	0.15	0.16	0.17	0.18
Derivative of lift to the pitch rudder angle	0.88	0.89	0.91	0.93	0.96	1.01
Derivative of pitch moment factor to the angle of attack	−0.87	−0.84	−0.79	-0.73	−0.61	−0.45
Pitch moment factor coefficient at zero angle of attack	0.06	0.06	0.06	0.06	0.07	0.08
Derivative of pitch moment factor to the pitch rudder angle	−2.99	−3.04	−3.10	−3.17	−3.29	−3.40
Derivative of the drag coefficient to the angle of attack	0.48	0.27	0.19	0.13	0.09	0.08
Zero lift drag coefficient	0.027					
Zero lift angle of attack (°)	−1.66					
Lift-induced drag coefficient	0.0937					
Wing reference area (m^2)	0.8319					
Gliding UUV mass (kg)	256.4					

Table 4 Gliding UUV thrust (N) at different altitudes and velocities

Altitudes (m)	0.3*Ma*	0.4*Ma*	0.5*Ma*	0.6*Ma*	0.7*Ma*	0.8*Ma*
3000	575	563	630	663	648	719
4000	542	531	527	539	588	650
5000	505	496	493	495	516	571
6000	453	446	444	446	453	499
7000	396	389	387	389	396	435
8000	343	338	336	338	343	378

is the horizontal distance of the rocket launch; g_o is the average gravitational acceleration of the Earth; m is the rocket mass; u_e represents the effective propulsion velocity of the rocket; S_a is the outlet area of the engine nozzle; P_r represents the actual pressure of the rocket; P_0 is the standard atmospheric pressure; C_{Xr} is the drag coefficient of the rocket (which is related to the Mach number); m_0 represents the initial mass of the rocket (i.e., the mass with full fuel); $\dot{m}$ represents the mass flow of the rocket fuel.

3.2 Dynamic model of the rocket in the release stage

In the release stage, the main task of the rocket is to reduce the velocity and release the gliding UUV. In the actual process, the entire release stage is very complex, involving the activation of the deceleration device and the release of the gliding UUV. Moreover, the operation time is very short. Therefore, this study mainly investigates the air flight trajectory of the gliding UUV with less emphasis on the deployment and release processes. The landing point, velocity, and final position of the rocket and gliding UUV are mainly investigated. In this study, the deceleration device is considered a rigid body, with the initial trajectory parameters of the gliding UUV in the conversion stage as the primary focus. The equations of the release stage are presented as follows:

$$\begin{cases} \dfrac{\mathrm{d}v_r}{\mathrm{d}t} = -g\sin\theta_r - a_X \\ \dfrac{\mathrm{d}\theta_r}{\mathrm{d}t} = -\dfrac{g_r\cos\theta_r}{v_r} + \dfrac{v_r\cos\theta_r}{r_E + h_d + h_r} \\ \dfrac{\mathrm{d}h_r}{\mathrm{d}t} = v_r\sin\theta_r \\ \dfrac{\mathrm{d}R_r}{\mathrm{d}t} = v_r\cos\theta_r \\ a_X = \dfrac{1}{2}\rho v^2 C_{Xj} S/m_r \end{cases} \tag{2}$$

where C_{Xj} represents the drag coefficient of the deceleration device and is related to the Mach number.

3.3 Dynamic model of the gliding UUV

The trajectory stages associated with the gliding UUV are the conversion, glide, and water entry stages, respectively. The dynamic models of the gliding UUV in these three trajectory stages are consistent. Both the conversion and glide stages of the UUV are program-controlled trajectories.

$$\begin{cases} \dfrac{\mathrm{d}v}{\mathrm{d}t} = \dfrac{T\cos\alpha - X}{m} - g\sin\theta \\ \alpha = \dfrac{1}{n_y^\alpha}\left(\dfrac{v}{g}\dfrac{\mathrm{d}\theta}{\mathrm{d}t} + \cos\theta - n_{y,\alpha=0}\right) \\ \dfrac{\mathrm{d}x}{\mathrm{d}t} = v\cos\theta \\ \dfrac{\mathrm{d}y}{\mathrm{d}t} = v\sin\theta \\ \theta = \theta_*(t) \\ X = \dfrac{1}{2}\rho v^2 C_X S \\ n_y = n_y^\alpha\alpha + n_{y,\alpha=0} \\ n_y^\alpha = \dfrac{1}{mg}\left(P + Y^\alpha - \dfrac{m_z^\alpha}{m_z^{\delta_z}}Y^{\delta_z}\right) \\ n_{y,\alpha=0} = \dfrac{1}{mg}\left(Y_0 - \dfrac{m_{z0}}{m_z^{\delta_z}}Y^{\delta_z}\right) \\ Y^\alpha = \dfrac{1}{2}\rho v^2 C_y^\alpha S \\ Y^{\delta_z} = \dfrac{1}{2}\rho v^2 C_y^{\delta_z} S \end{cases} \tag{3}$$

where v represents the velocity of the gliding UUV; T is the thrust of the gliding UUV; X represents the gliding UUV's drag; α is the angle of attack; m is the mass of the gliding UUV; θ is the trajectory inclination angle; C_X is the drag coefficient of the gliding UUV, S is the reference area of the gliding UUV; n_y represents the normal overload; n_y^α represents the normal overload at the angle of attackα; $n_{y,\alpha=0}$ represents the normal overload at a zero angle of attack; x is the horizontal distance of the gliding UUV from each initial position; y is the altitude of the gliding UUV; Y^α represents the derivative of lift to the angle of attack α; Y^{δ_z} represents the derivative of lift to the pitch rudder angle δ_z; m_z^α represents the derivative of the pitch moment factor to the angle of attack α; $m_z^{\delta_z}$ represents the derivative of the pitch moment factor to the pitch rudder angle δ_z; C_y^α is the lift curve slope; $C_y^{\delta_z}$ is the derivative of the lift coefficient to the pitch rudder angle δ_z.

During the conversion and water entry stages, thrust coordination is required to change the gliding UUV's attitude. In comparison, the thrust value is 0 in the glide stage.

To achieve the desired trajectory and attitude for the

gliding UUV, this work employs the rudder deflection angle δ_z as the control input. A RHC receding horizon optimization algorithm (Ahmed and Sheltami, 2024) is adopted, which generates locally optimal control commands for the gliding UUV over a finite time horizon T by solving constrained optimization problems online. $\delta_z(t)$ represents the required rudder deflection adjustment at the next time step.

The state of the gliding UUV at time t is expressed by the following equation:

$$\eta(t) = \left[x(t), y(t), v(t), \theta(t)\right] \tag{4}$$

Over the time horizon $[t, t+T]$, the optimization criterion $\min J(t, \eta(t), \delta_z(t))$, minimizing the value of the cost function $J(t, \eta(t), \delta_z(t))$, is solved subject to constraints to obtain a locally optimal control command $\delta_z(t)$. The specific formulation of the cost function is presented below:

$$\begin{cases} J(t, \eta(t), \delta_z(t)) = \\ \int_t^{t+T} r_1 \Delta x^2(\tau) + r_2 \Delta y^2(\tau) + r_3 \Delta\theta^2(\tau)\, \mathrm{d}\tau \\ \Delta x = x(t) - x_d(t) \\ \Delta y = y(t) - y_d(t) \\ \Delta\theta = \theta(t) - \theta_d(t) \end{cases} \tag{5}$$

where $x_d(t)$ and $y_d(t)$ represent the desired position at time t, $\theta_d(t)$ represents the desired trajectory inclination angle at time t, and r_1, r_2, and r_3 represent the weighting coefficients.

The constraints for the optimization problem are expressed by the following equation:

$$\begin{cases} \dot{\eta}(t) = F(\eta(t), \delta_z(t)) \\ \eta(0) = \eta_0 \\ \delta_z(t) \in \left[-\delta_{zm}, \delta_{zm}\right] \\ v(t) \in \left[v_{\min}, v_{\max}\right] \end{cases} \tag{6}$$

where $\dot{\eta}(t) = F(\eta(t), \delta_z(t))$ denotes the constraint that the UUV must satisfy in the kinematic model given in Equation (3). $\eta(0) = \eta_0$ denotes the initial state of the gliding UUV upon entry into the conversion stage. $\delta_z(t) \in \left[-\delta_{zm}, \delta_{zm}\right]$ represents the rudder deflection angle constraint imposed by mechanical structural limits on the gliding UUV's tail rudder, specified as 20° in this study. $v(t) \in \left[v_{\min}, v_{\max}\right]$ is the permissible velocity range for the gliding UUV, determined by conversion stage operational requirements. This range varies across the conversion, gliding, and water entry stages.

The optimal control command $\delta_z(t)$ computed over the time horizon Tusing the RHC algorithm is applied to the gliding UUV. Subsequently, the gliding UUV's state is remeasured at the next time step, and the optimization procedure repeats iteratively until mission completion.

3.4 Trajectory design of the gliding UUV in the conversion and glide stages

The conversion stage of the gliding UUV is the most complex and challenging in the whole flight process. Because the flight is controlled by a programmed trajectory, the trajectory curve of the gliding UUV in the conversion stage must be studied, and a certain parameter that varies with time must then be selected for storage in the program. To control the program trajectory section easily, the pitch angle, altitude, or trajectory inclination angle is generally used as a parameter, with pitch angle control being the simplest and most convenient. This study uses the trajectory inclination angle as the design variable to intuitively design a more reasonable and concise trajectory. In practice, the trajectory inclination angle and the pitch angle can be directly transformed into each other using standard kinematic relationships.

In the conversion stage, the entire flight process is conducted automatically by the program. The velocity and angle of the gliding UUV change constantly throughout the entire stage. The overall flight trajectory is shown in Figure 4.

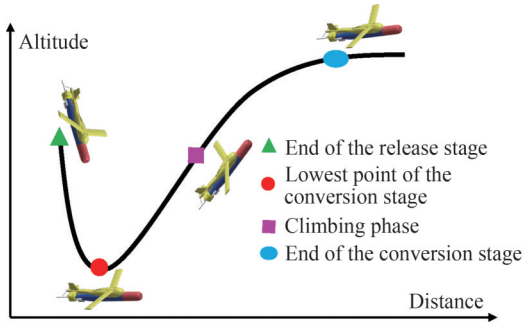


Figure 4 Preset flight path of the conversion stage

As shown in Figure 4, at the end of the release stage, the gliding UUV dives down as the trajectory inclination angle approaches −90°. Because of the release position of the rocket, the pitch angle of the gliding UUV is also close to −90°. Controlled by internal procedures, the trajectory inclination angle gradually turns to 0°. At this moment, the trajectory inclination angle control program begins to work, and the gliding UUV begins to climb up. Then, the trajectory inclination angle increases gradually. At the lowest point of the conversion stage, the trajectory inclination angle becomes 0° and then increases gradually. The gliding UUV then climbs up steadily. When the gliding UUV stabilizes at a certain altitude, its attitude begins to flatten, and the trajectory inclination angle finally returns to around 0°. The gliding UUV then enters the glide stage.

To ensure a smooth transition from the lowest point to

the climbing phase, the trajectory inclination angle is designed using a piecewise quadratic function, as shown in Figure 5. Here, θ_0 is the trajectory inclination angle of the release stage, and θ_1 is the designed maximum trajectory inclination angle. t_0 represents the beginning of the conversion stage, t_1 represents the moment of the maximum trajectory inclination angle of the gliding UUV in the climbing phase, and t_2 represents the end of the conversion stage.

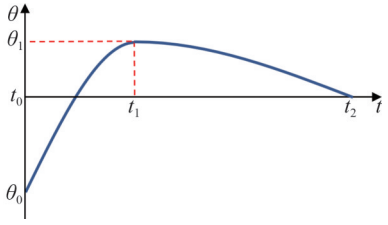


Figure 5 Design of the trajectory inclination angle in the conversion stage

The initial trajectory parameter of the gliding UUV in the glide stage is obtained from the end point of the conversion stage. A fixed trajectory inclination angle is designed, and the free glide performance of the gliding UUV can be observed. The objective of the glide stage is to continuously reduce both the glide altitude and velocity in preparation for the subsequent water entry stage.

4 Simulation results and analysis

4.1 Rocket flight stage

Combined with all the relevant parameters given by the overall design department, the rocket flight time is set to 230 s, the engine working time is 30 s, and the initial launch angle is 70.5°. For comparison with the release stage hereinafter, the simulation is extended to 250 s. The numerical integration method utilizes the fourth-order Runge–Kutta method. The results are shown in Figure 6.

As shown in Figure 6, the structure, airborne equipment, and sensors should be designed to withstand more than 20 g of axial overload because of the high flight velocity and significant axial overload. As the reentry velocity into the dense atmosphere reaches up to 5*Ma* to 6*Ma*, aerodynamic thermal protection during deceleration should be considered. Protective covers and other means should be used to avoid severe aerodynamic heating.

To study the impact of the initial launch angle on the rocket's flight range, the trajectory is simulated under initial launch angles of 75°, 70.5°, and 65°, respectively (Figure 7). The comparison indicates variations in the trajectory of the rocket. In actual operations, the launch angle can be flexibly adjusted according to the target distance.

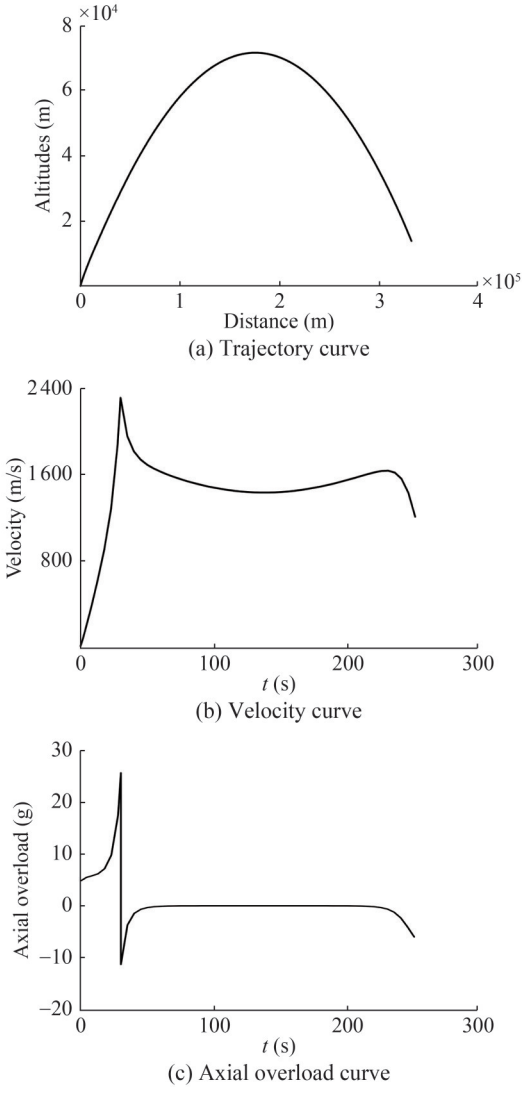


Figure 6 Curves of the flight stage

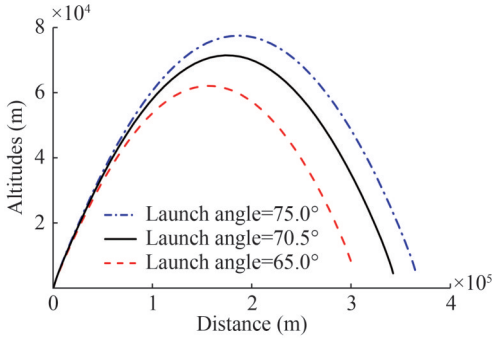


Figure 7 Trajectory curves of the flight stage at different launch angles

Figure 8 presents trajectories under varying thrust conditions. Increased thrust magnitudes correspond to higher peak altitudes of rocket flight. Under identical simulation durations, enhanced thrust levels also yield greater penetra-

tion ranges. In practical deployment scenarios, rocket thrust should be optimally determined according to the specified penetration range requirements and maximum altitude constraints.

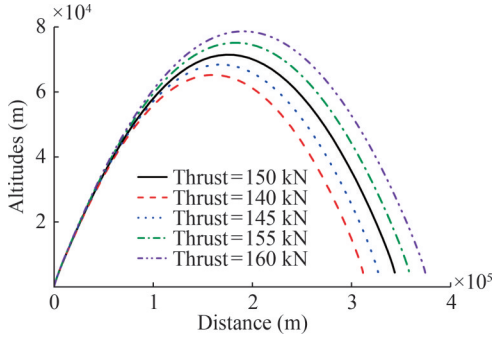


Figure 8 Trajectory curves of the flight stage at different thrusts

Figure 9 demonstrates the effect of various drag coefficients on the rocket flight trajectory. The drag coefficient is governed not only by the rocket's configuration but also by its flight Mach number. Here, $C_{Xr}0$ denotes the baseline set of Mach-number-dependent drag coefficients for the rocket's design trajectory, whereas $C_{Xr}1$, $C_{Xr}2$, and $C_{Xr}3$ represent three progressively increasing alternative sets of Mach number-dependent drag coefficients. $C_{Xr}1$ consistently exceeds $C_{Xr}0$ in terms of magnitude across the Mach number regime, whereas sets $C_{Xr}2$ and $C_{Xr}3$ remain below $C_{Xr}0$. Figure 9 indicates that progressive increases in drag coefficient correspond to reductions in both the peak altitude and penetration range of the rocket. In practical engineering applications, distinct aerodynamic configurations correspond to specific drag coefficients. The selection of drag coefficient values should be governed by mission-specific altitude requirements, range specifications, and payload capacity, thereby determining optimal aerodynamic profiles and lifting surface configurations.

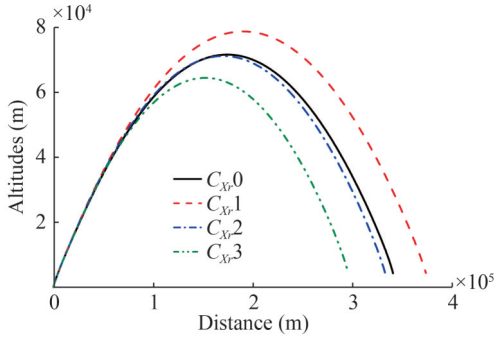


Figure 9 Trajectory curves of the flight stage at different drag coefficients

4.2 Release stage

The trajectory parameters at the end of the rocket flight stage are used as the initial parameters of the rocket release stage for simulation. The altitude is 20.6 km, the angle is −28.7°, the velocity is 1 640 m/s, and the release stage time is 60 s. The results are shown in Figure 10. The distance of the rocket in the release stage is 13 km, and the height drops from 20 km to about 7 000 m. Because of the deceleration device, the rocket's velocity drops rapidly in the first 10 s, with the final velocity reduced to 150 m/s. The trajectory inclination angle also changes from −28.7° to −85°. In the initial release stage, the maximum value of the axial overload is 20g. This significant overload results from the sudden opening of the deceleration brake to reduce the overall velocity of the rocket. The axial overload is gradually reduced by continuously adjusting the trajectory inclination angle of the rocket. By comparing the terminal data of the rocket flight stage, the release stage of the rocket provides an appropriate velocity and angle for the separation of the gliding UUV from the rocket. Without the release stage, the UUV attains an excessively high velocity during release, resulting in an overly small trajectory inclination angle. This produces a relatively flat overall attitude, leading to instability and vulnerability to environmental influence.

By varying the time allocation between the flight and release stages, the rocket's trajectory results under different flight schemes are obtained. In Scheme 1, the rocket flight stage lasts 230 s and the release stage 60 s; in Scheme 2, the flight and release durations are 220 and 75 s, respectively; in Scheme 3, they are 210 and 90 s, respectively. The simulation results are given in Table 5.

As shown in Table 4, the longer the flight period, the lower the altitude of the release stage and the greater the corresponding maximum axial load. Conversely, the shorter the flight period, the higher the initial altitudes of the release period, where the air density is lower. This leads to a relatively small dynamic pressure. Therefore, as the flight period decreases, the maximum axial load corresponding to the rocket gradually decreases.

The trajectory parameters at the end of the deceleration stage are almost the same. The comparison results indicate that the initial altitude of the release stage strongly influences the flight performance of the rocket. Thus, when the time constraint is not too high, the initial altitude of the release stage can be appropriately raised to reduce the axial load. However, an excessively high initial altitude of the release stage is counterproductive: the longer the release time, the greater the risk of the rocket and gliding UUV being intercepted and hit by enemy anti-aircraft weapons.

4.3 Conversion stage

The terminal parameters of the rocket release stage are considered the initial parameters of the conversion stage. The initial altitude is 7 000 m, the initial velocity is 150 m/s, the initial trajectory inclination angle is −85°, the time of

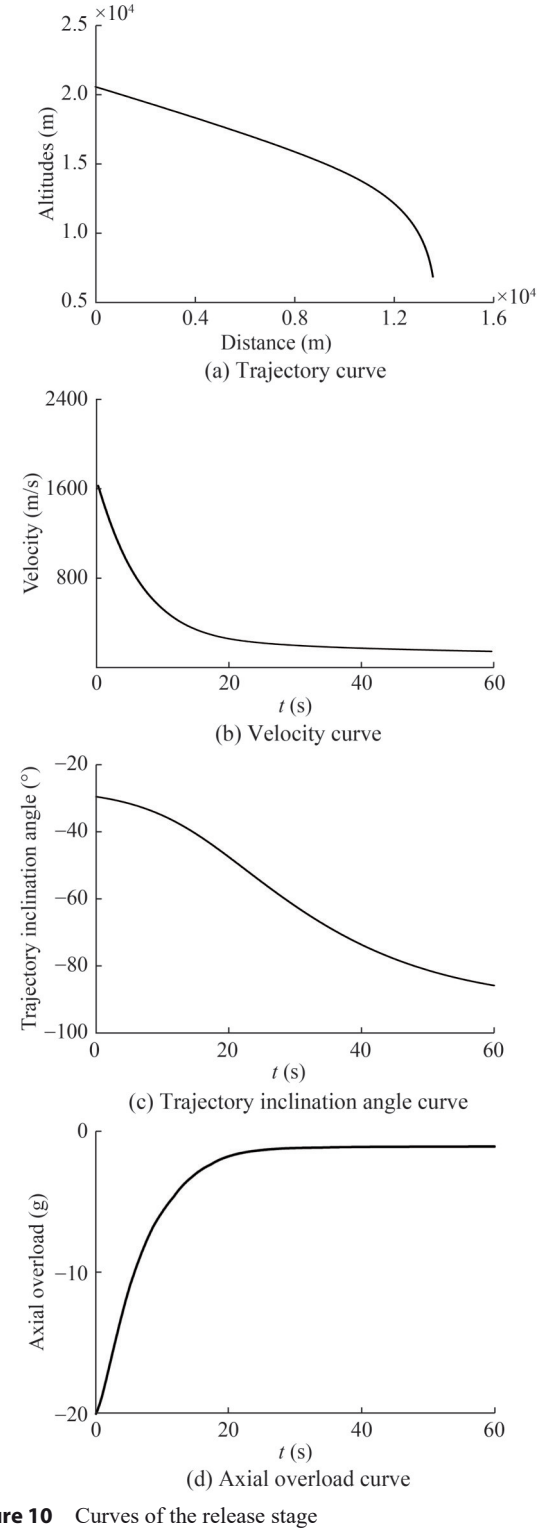


Figure 10 Curves of the release stage

the conversion stage is 110 s, and the designed maximum trajectory inclination angle is 12°. To exit the vertical dive promptly and reach the minimum safe altitude of the gliding UUV, the maximum trajectory inclination angle is scheduled to occur at 12 s. When the trajectory inclination angle turns to 0, the conversion stage ends. During the conversion stage, the gliding UUV engine assists in its attitude change. The thrust data are obtained from Table 3, and the simulation results of the conversion stage are shown in Figure 11.

Table 5 Comparison results for the three schemes

Parameter	Scheme 1	Scheme 2	Scheme 3
Penetration distance (km)	343.5	339.6	337.2
Conversion altitudes (m)	7000	7400	8500
Terminal trajectory inclination angle (°)	−85	−87.4	−88.6
Velocity of conversion (m/s)	150.4	161.3	168.5
Maximum axial overload (g)	−20	−14.6	−6.2

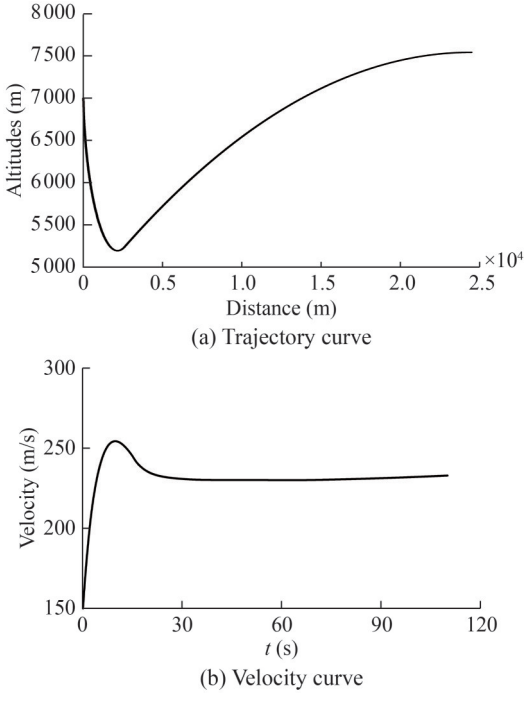


Figure 11 Curves of the conversion stage

As shown in Figure 11(a), the conversion trajectory curve aligns with the expected design trajectory, which is reasonable and reliable. The final altitude of the flight is kept at 7 500 m. The end of the conversion trajectory is relatively stable, transitioning the gliding UUV into the glide stage gradually. As shown in Figure 11(b), because of the dual effect of gravity and thrust, the velocity of the gliding UUV increases continuously in the early stage of conversion and then reaches its maximum when the trajectory inclination angle reaches 0. As the trajectory inclination angle increases, the gliding UUV presents a climbing attitude, and the velocity stabilizes after a slight decrease.

To investigate the effect of different initial velocities on

the conversion trajectory, trajectory results at different conversion velocities are presented. To facilitate convenient comparison and analysis, the initial conversion altitude is set at 7 000 m.

Figure 12 compares the conversion trajectories when the initial velocities are set to 120, 150, 180, and 210 m/s. The higher the conversion velocity, the greater the altitude loss, and the corresponding minimum safe altitude may not be guaranteed. The lower the conversion rate, the higher the altitude after final stabilization, which may exceed the upper limit of the gliding UUV. The initial velocity is determined by accounting for the minimum safe altitude, the upper limit, and the initial release altitude.

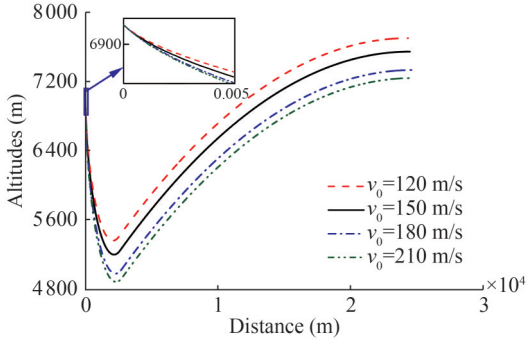


Figure 12 Trajectory curves at different initial velocities

Figure 13 comparatively presents the design trajectory, along with resultant trajectories under RHC, RHC with disturbance scenarios, and proportional–integral–derivative (PID) control algorithms. The implemented RHC algorithm accurately tracks the reference trajectory. The controlled flight path exhibits close conformity to the design profile, with minimal deviation at the perigee altitude and stable terminal convergence near the prescribed endpoint elevation. Incorporating practical atmospheric disturbances affecting the gliding UUV, the RHC algorithm maintains effective reference trajectory tracking despite applied external perturbations. Although the simulation results exhibit minor deviations from the design terminal altitude, they demonstrate the controller's robust disturbance rejection capability. While the PID control algorithm ultimately achieves marginal compliance with design requirements, it exhibits significantly larger deviations compared with the RHC approach. Measurable discrepancies are observed at both the perigee altitude and in the steady-state terminal condition, resulting in comparatively inferior overall performance relative to the RHC controller.

4.4 Glide stage

The glide stage is mainly considered the transition between the conversion and water entry stages. In this paper, a programmed trajectory method is utilized, and the trajectory inclination angle is set to −10°, adjusted from 0° to

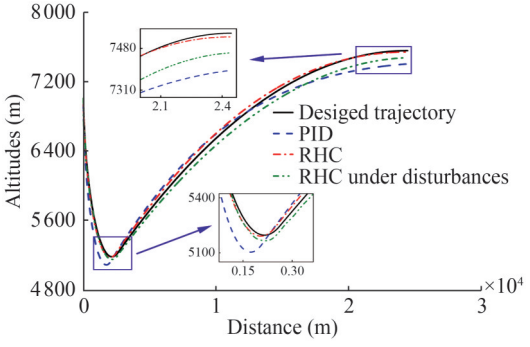


Figure 13 Trajectory curves under comparative control algorithms

−10° within 2 s at the end of the conversion stage. The gliding UUV maintains a downward flight attitude without power in the glide stage. The initial altitude is 7 500 m, the initial velocity is 230 m/s, and the glide time is 220 s. The simulation results are illustrated in Figure 14. During gliding, the altitude of the gliding UUV and the velocity decrease continuously. The whole gliding distance is about 42 km, which further increases the distance of the gliding UUV. The terminal altitude of the gliding stage is 70 m, and the velocity is about 160 m/s, satisfying the conditions for the water entry stage.

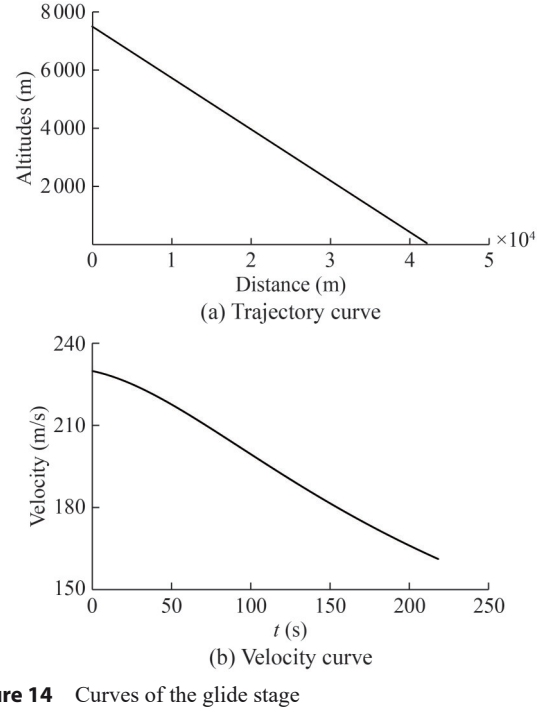


Figure 14 Curves of the glide stage

4.5 Water entry stage

The water entry stage is the last phase of the gliding UUV's flight trajectory and is the most important for ensuring that the UUV enters the water safely. Generally, the water entry angle of the UUV should be controlled

within the range of −30° to −80°, and the velocity should be controlled below 50 m/s (Wang, 2010). However, the velocity at the end of the glide stage is still very high. Auxiliary deceleration devices are thus required before water entry. Multiple deceleration methodologies, including parachutes, deceleration brakes, and a rocket reverse thrust system, must be employed. Parachute deployment necessitates protracted canopy inflation and deceleration phases, extending airborne exposure duration that degrades the UUV's low-observability characteristics. However, concurrent parasitic oscillations during descent impose substantial terminal impact loads on the UUV structure. Moreover, deceleration brakes impose significant spatial constraints that complicate integration onto the gliding UUV: they typically require hydraulic, pneumatic, or electromechanical actuation systems, which notably elevate control system complexity. Meanwhile, although rocket reverse thrust systems reduce UUVs' effective payload capacity, they offer significantly shorter deceleration times and superior controllability. These systems enable rapid velocity reduction under lower deceleration overload conditions. Thus, this paper uses a miniature rocket reverse thrust system to decelerate the gliding UUV (Xing, 2012). To achieve center-of-mass control, solid rocket motors are selected as thrusters. A dual-thruster configuration is employed, with both propulsors mounted symmetrically about the longitudinal axis on the UUV's lateral surfaces, delivering reverse thrust for a controlled 3-s duration. The relevant simulation conditions are given in Table 6, and the final simulation results of the water entry stage are shown in Figure 15.

Table 6 Water entry condition setting

Parameter	Numerical value
Initial altitude (m)	70
Initial velocity (m/s)	167
Reverse thrust (N)	−14000
Reaction time of the reverse thrust (s)	3
Installation position of the reverse thrust rocket (mm)	10 (below the centroid)

As substantiated by Figure 15(a), after flying 190 m, the gliding UUV reaches the water entry point. Figure 15(b) evinces that the velocity decreases rapidly in the early stage, reaches a basic equilibrium with the drag in the late stage, and then stabilizes at 33.3 m/s. Figure 15(c) shows a downward trend from the end of the glide stage, and the pitch angle before the final entry is −72°. The velocity and pitch angle satisfy the corresponding requirements of water entry, and the trajectory of the entire water entry stage is reasonable and reliable.

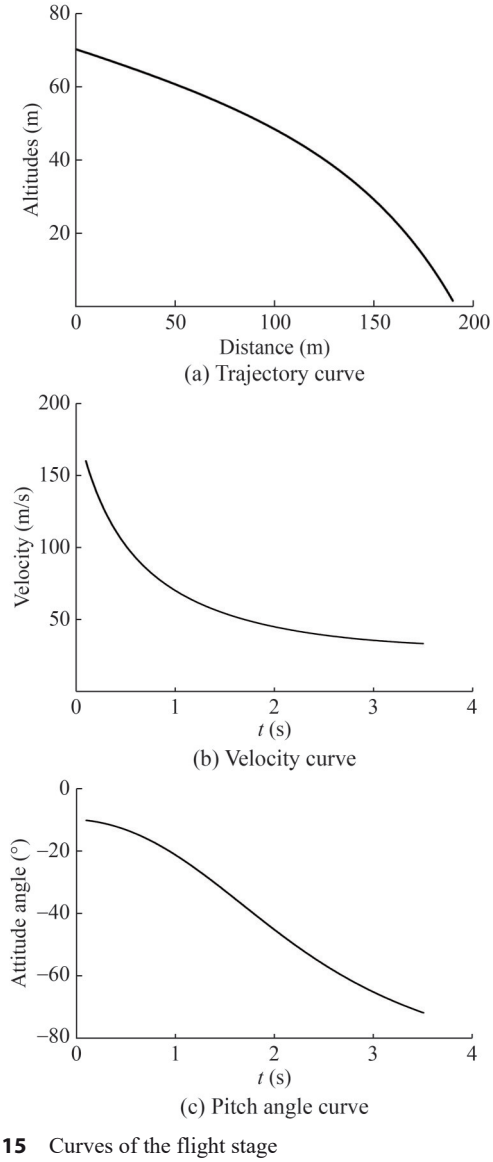


Figure 15 Curves of the flight stage

4.6 Full flight trajectory

The trajectory curve of the entire process—from penetration platform launch to water entry—is shown in Figure 16. The velocity and acceleration curves of the entire flight are shown in Figures 17 and 18, respectively, with respect to distance and time. The total flight time of the gliding UUV is 633.5 s, and the flight distance is 410 km. The overall trajectory aligns with the expected operational objectives, improving the UUV's mobility, long-distance penetration, and strike capability.

In Figures 17 and 18, the segment from point *a* to point *d* represents the flight stage. The velocity and acceleration of the rocket increase continuously under the thrust of the fuel. At point *b*, the rocket's engine turns off, causing the acceleration to drop to a minimum instantaneously. The velocity gradually decreases, but the altitude still increases.

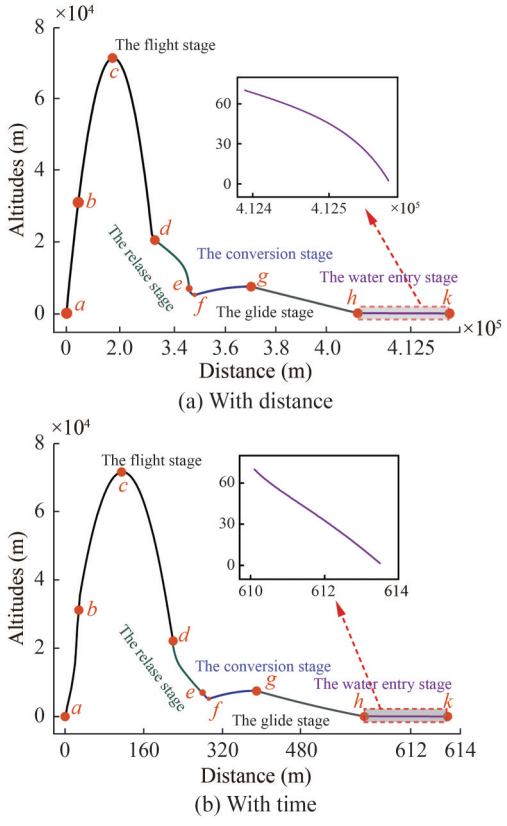


Figure 16 Trajectory curves of the entire flight

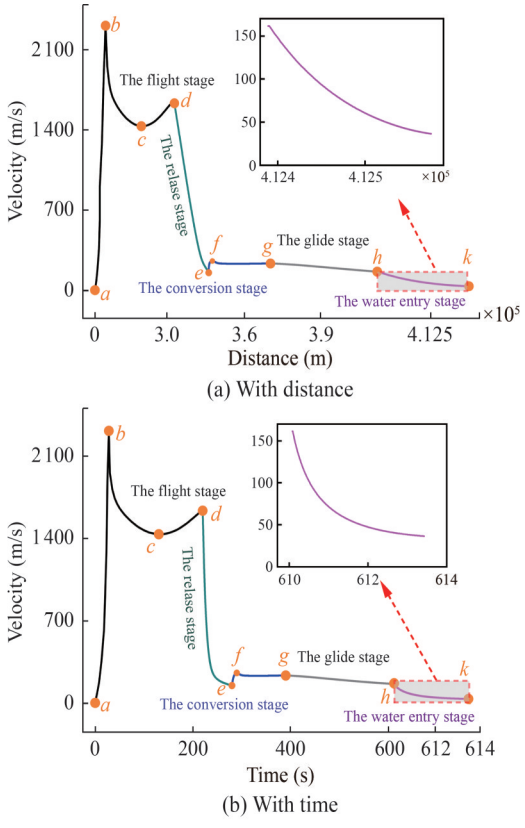


Figure 17 Velocity curves of the entire flight

At point *c*, the height reaches its maximum value when the velocity is at a local minimum value, and the acceleration is 0. Subsequently, the velocity slightly increases because of the effect of gravity.

The segment from point *d* to point e represents the release stage. After opening the deceleration brakes, the rocket's velocity decreases rapidly, and the acceleration suddenly drops to its minimum value. At the end of the release stage, the acceleration gradually becomes 0, and the velocity changes slowly, facilitating conditions for the safe separation of the gliding UUV.

The segment from point *e* to point *g* represents the conversion stage. After separation, the gliding UUV engine starts, and the spacecraft accelerates downward at this time. At point *f*, the UUV reaches the lowest point of the conversion stage, and the velocity and acceleration gradually stabilize.

The segment from point *g* to point *h* represents the glide stage. During gliding, the altitude and velocity continuously decrease, whereas the acceleration varies within a small range.

The segment from point *h* to point *k* represents the water entry stage. The velocity of the gliding UUV decreases rapidly under the action of the miniature rocket reverse thrust system, and the acceleration eventually becomes 0.

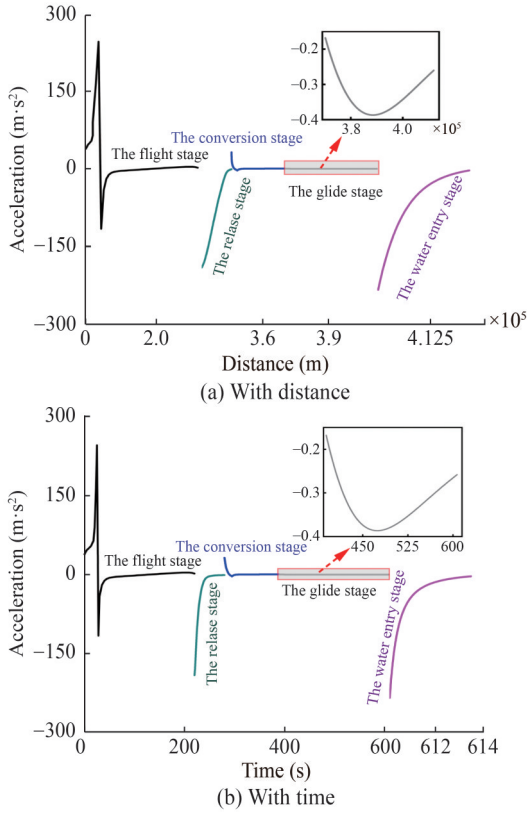


Figure 18 Acceleration curves of the entire flight

5 Conclusions

5.1 Main conclusions

To improve maneuverability and penetration capability and achieve long-distance targets, this paper proposes an overall flight scheme for a high-altitude, long-distance gliding UUV. This paper studies the trajectory planning problem from rocket launch to UUV water entry, achieving smooth gliding UUV conversion and meeting safe water entry requirements. Detailed simulation analysis is conducted for each section to verify the scheme's feasibility and provide a basis for the overall demonstration. The UUV can be rapidly deployed and has high penetration performance, enhancing its ability to engage in long-distance trans-medium combat. For different aircraft or gliding UUVs, new trajectory results can be obtained simply by changing their overall parameters in the simulation. The method proposed in this paper thus presents good universality.

1) Considering the characteristics of the flight plan of the high-altitude, long-distance gliding UUV, dynamic models of all flight stages of the rocket and the gliding UUV are established. Moreover, stable and reliable trajectories of the conversion and glide stages are designed. The rocket can deploy the gliding UUV for more than 300 km in 290 s in the trajectory simulation.

2) Using the same initial parameters of the conversion stage, the results of different time allocations between the flight and release stages of the rocket are compared. The earlier release time produces a lower axial load, which is conducive to the safe release of the gliding UUV.

3) By designing a piecewise quadratic trajectory inclination angle to complete the UUV's smooth conversion after the rocket's release. The feasibility of the conversion stage trajectory design is validated using an RHC algorithm. The effect of different initial gliding UUV velocities on the conversion stage is investigated. The greater the initial velocity, the greater the loss of altitude. The altitude loss caused by each initial velocity cannot be greater than the minimum safety altitude required in actual combat.

4) The glide stage provides a smooth transition from the conversion stage to the water entry stage. The pitch angle is −72°, and the UUV's velocity is 33.3 m/s before water entry, satisfying the conditions of safe trans-medium entry.

5.2 Limitations and future work

1) This research specifically focused on axisymmetric air-deployed UUV configurations. Future work should extend validation to alternative UUV geometries upon acquiring experimentally determined aerodynamic parameters. Concurrent investigations should address diverse operational theaters to enhance the versatility and applicability of the proposed methodology.

2) The current research analyzed the feasibility of a flight scheme and the rationality of the trajectory of a high-altitude, long-distance gliding UUV in general. In the future, the dynamic response and intelligent control strategy of the gliding UUV at each stage should be studied in detail to further improve the UUV's performance.

3) Owing to the extended penetration range afforded by high-altitude, long-distance gliding UUVs, this investigation focused on their vertical-plane kinematics. Subsequent research should explore multi-degree-of-freedom dynamics encompassing yaw, roll, and coupled motion regimes to enhance engineering applicability.

Funding Supported by the National Natural Science Foundation of China (Grant Nos. U24B20115, 52471346, 51909206), Natural Science Basic Research Plan in Shaanxi Province of China (Grant No. 2024JC-YBMS-300), China Postdoctoral Science Foundation (Grant No. 2021M692616), and Fundamental Research Funds for the Central Universities (Grant No. 31020200QD044).

Competing interests The authors have no competing interests to declare that are relevant to the content of this article.

References

Ahmed G, Sheltami T (2024) Receding horizon and optimization-based control for UAV path planning with collision avoidance. Procedia Computer Science 251: 15-22. https://doi.org/10.1016/j.procs.2024.11.079

Chen C, Chen X, Hang P (2025a) Personalized longitudinal motion planning based on a combination of reinforcement learning and imitation learning. Green Energy and Intelligent Transportation: 100321. https://doi.org/10.1016/j.geits.2025.100321

Chen G, Zhang W, Qi L, Xue H, Huang W, Hu J (2024) Constrained multi-objective trans-media maneuver trajectory optimization for morphing unmanned aerial-underwater vehicles. Ocean Engineering 299: 117380. https://doi.org/10.1016/j.oceaneng.2024.117380

Chen H, Sun Q, Cheng S (2025b) Design and simulation analysis of the aerial track of trans-medium glider. Proceedings of 4th 2024 International Conference on Autonomous Unmanned Systems (4th ICAUS 2024), Singapore, 526-539

Chen J, Wang Z, Cao X, Zhang Q, Cai W (2020) Trajectory design of high-altitude gliding torpedo based on optimal guidance law. Journal of Unmanned Undersea Systems 28(3): 278-283+290

Ding Y, Wang X, Bai Y, Cui N (2020) Novel anti-saturation robust controller for flexible air-breathing hypersonic vehicle with actuator constraints. ISA Transactions 99: 95-109. https://doi.org/10.1016/j.isatra.2019.09.010

Fan X, Bai X, Jiang Z, Zhang S (2022) Dynamic performance test and system identification of air rudder for boost-glide aircraft. Springer Aerospace Technology, Springer, Singapore, 26-42. https://doi.org/10.1007/978-981-16-6640-7_3

Guo J, Liang L, Guo Z (2024a) Combined-cycle propulsion-involved trajectory optimization and performance-driven attitude control for aerospace plane during the ascent phase. IEEE Transactions on Intelligent Transportation Systems 25(12): 21086-21096. https://doi.org/10.1109/TITS.2024.3470528

Guo Z, Cao S, Yuan R, Guo J, Zhang Y, Li J, Hu G, Han Y (2024b) Reinforcement learning-based integrated decision-making and control for morphing flight vehicles under aerodynamic uncertainties. IEEE Transactions on Aerospace and Electronic Systems 60(6): 9342-9353. https://doi.org/10.1109/TAES.2024.3440969

Hu G, Cheng M, Houssein EH, Jia H (2025a) CMPSO: A novel co-evolutionary multigroup particle swarm optimization for multi-mission UAVs path planning. Advanced Engineering Informatics 63: 102923. https://doi.org/10.1016/j.aei.2024.102923

Hu Y, Liu Z, Jiang C, Jing W, Gao C (2025b) Maneuver mode parametric modeling based on trajectory curve evolution laws for hypersonic glide vehicles. Aerospace Science and Technology 157: 109856. https://doi.org/10.1016/j.ast.2024.109856

Li D (2017) Preliminary and trajectory optimization designing of rocket carrying and launching UAV. Master thesis, Nanjing University of Aeronautics and Astronautics, Nanjing

Li Y (2018) Research on aerodynamic shape multidisciplinary optimization design method of high-altitude glide UUV. PhD thesis, Northwestern Polytechnical University, Xi'an

Liu H, Pan G, Du X (2014) Estimation and simulation of aerodynamic parameters of high-altitude long-distance gliding UUV. Journal of Northwestern Polytechnical University 32(2): 246-250

Liu S, Bai J (2021) Exploration of high-altitude dynamic soaring based on six-degree-of-freedom model. Journal of Northwestern Polytechnical University 39(4): 703-711. https://doi.org//10.1051/jnwpu/20213940703

Lui DG, Tartaglione G, Conti F, Tommasi GD, Santini S (2023) Long short-term memory-based neural networks for missile maneuvers trajectories prediction. IEEE Access 11: 30819-30831. https://doi.org/10.1109/ACCESS.2023.3262023

Pan G, Liu H, Du X (2012) Exploring feasibility of low altitude penetration of high-altitude long-distance gliding UUV. Journal of Northwestern Polytechnical University 30(3): 417-421

Pan G, Liu H, Du X (2013) Simulation and analysis of deceleration segment of high-altitude long-distance gliding UUV. Fire Control & Command Control 38(4): 158-161

Pan G, Wu W, Mao Z, Huang Q (2009) Key technologies about complete trajectory simulation for high altitude long-range gliding torpedo. Torpedo Technology 17(4): 10-15

Qi W, Cheng S, Li K (2022) Research progress of hypersonic vehicle and propulsion system. Technology Innovation and Application 12(31): 18-21

Tang J, Wang G, Wu G, Sun Y, Gu L, Rui X (2025) Launch dynamics modeling and simulation of box-type multiple launch rocket system considering plane clearance contact. Defence Technology 47: 105-123. https://doi.org/10.1016/j.dt.2024.12.016

Wang C, Xu H, Ma G, Sun L (2024a) Research progress of cutting-edge technologies of trans-medium vehicle dynamics. Journal of Unmanned Undersea Systems 32(3): 384-395

Wang H, Tong S, Wang A, Zhang W, Hu Z, Peng Z (2024b) Heterogeneous cross domain coordinated control of ASV-AUV system for maritime search and rescue. Ocean Engineering 306: 117950. https://doi.org/10.1016/j.oceaneng.2024.117950

Wang S, Song S, Duan G, Zhang K (2012) An effective design and simulation of control system for high altitude long-range gliding torpedo. Journal of Northwestern Polytechnical University 30(5): 706-711

Wang Y (2010) Performance description coefficient of airborne torpedo and deep-mine during water-entry impact. Aeronautical Computing Technique 40(6): 14-17

Wei W, Wang J, Fang Z, Chen J, Ren Y, Dong Y (2023) 3U: Joint design of UAV-USV-UUV networks for cooperative target hunting. IEEE Transactions on Vehicular Technology 72(3): 4085-4090. https://doi.org/10.1109/TVT.2022.3220856

Xing R (2012) Research on rocket booster technique for high altitude and long range glider UUV. Master thesis, Northwestern Polytechnical University, Xi'an

Xu H, Guedes Soares C (2025) Review of system identification for manoeuvring modelling of marine surface ships. Journal of Marine Science and Application 24(3): 459-478. https://doi.org/10.1007/s11804-025-00681-w

Yahi N, Matute J, Karimoddini A (2024) Receding horizon based collision avoidance for UAM aircraft at intersections. Green Energy and Intelligent Transportation 3(6): 100205. https://doi.org/10.1016/j.geits.2024.100205

Yan J, Lin J, Yang X, Chen C, Guan X (2025) Cooperation detection and tracking of underwater target via aerial–surface–underwater vehicles. IEEE Transactions on Automatic Control 70(2): 1068-1083. http://doi.org/10.1109/TAC.2024.3447976

Yang F, Xia G (2020) A finite-time 3D guidance law based on fixed-time convergence disturbance observer. Chinese Journal of Aeronautics 33(4): 1299-1310. https://doi. org/10.1016/j.cja.2020.01.001

Yao G, Li Y, Zhang H, Jiang Y, Wang T, Sun F, Yang X (2023) Review of hybrid aquatic-aerial vehicle (HAAV): Classifications, current status, applications, challenges and technology perspectives. Progress in Aerospace Sciences 139: 100902. https://doi.org/10.1016/j.paerosci.2023.100902

Ye J, Li C, Wen W, Zhou R, Reppa V (2023) Deep learning in maritime autonomous surface ships: Current development and challenges. Journal of Marine Science and Application 22(3): 584-601. https://doi.org/10.1007/s11804-023-00367-1

Yılmaz AN, Cihan M (2023) Modeling and simulation of pre-apogee trajectories for low altitude rockets. 2023 10th International Conference on Recent Advances in Air and Space Technologies (RAST), Istanbul

Zhang C, Yang F, Liu K, Xia G, Kang H, Niu Y, Lu C (2021) Development and key technology analysis of morphing trans-media aircraft. Astronautical Systems Engineering Technology 5(6): 9

Zhang J (2010) Research on integrative design and ballistic trajectory simulation for rocket-launch unmanned air vehicle. Master thesis, Northwestern Polytechnical University, Xi'an

Zhang K, Wen J, Gu L, Liang Y (2013) Optimal control design and simulation of high-altitude long-range glider UUV. Measurement & Control Technology 32(3): 66-69. DOI: 10.19708/j.ckjs.2013.03.017

Zhao Z, Zhao C, Ma A (2024) Development status and future prospects of trans-media aircraf. Missiles and Space Vehicles (2): 17-24

Zhao ZT, Huang W, Yan L, Yang YG (2020) An overview of research on wide-speed range waverider configuration. Progress in Aerospace Sciences 113: 100606. https://doi.org/10.1016/j.paerosci.2020.100606